Materials Science and Engineering A 528 (2011) 2982–2987

Contents lists available at ScienceDirect

Materials Science and Engineering A

journal homepage: www.elsevier.com/locate/msea

Dominant factor controlling the fracture mode in nanostructured Cu/Cr multilayer films

J.Y. Zhang, X. Zhang, G. Liu*, G.J. Zhang, J. Sun*

State Key Laboratory for Mechanical Behavior of Materials, Xi'an Jiaotong University, XianNing West Road 28, Xi'an 710049, PR China

ARTICLE INFO

Article history:
Received 21 November 2010
Accepted 14 December 2010
Available online 22 December 2010

Keywords:
Nanostructured multilayers
Fracture mode
Constraint effects
Length scale

ABSTRACT

It was recently suggested that the fracture mode in nanostructured metallic multilayer films (NMFs) is related to the strengthening mechanism. Here, based on extensive experimental examinations on the nanoscale damage of Cu/Cr NMFs with wide ranges of modulation period (from 10 nm to 250 nm) and modulation ratio (from 0.11 to 3.0), we conclude that the dominant factor controlling the fracture mode in NMFs is the constraint effect from the ductile layer on the brittle layer, rather than the strengthening mechanism. This constraint effect is quantitatively assessed using a fracture mechanism-based micromechanical model, which yields predictions in broad agreement with the experimental observations.

1. Introduction

Nanostructured metallic multilayer films (NMFs) represent a class of advanced engineering materials and attract much more attention recently owing to their unique properties [1–6]. Most NMFs with equal individual layer thickness (i.e., modulation ratio $\eta \sim 1$), involved in mechanical test, were found to exhibit a monotonic increase in strength/hardness with decreasing modulation period (λ) [7–13], which is because the nucleation and motion of dislocations are strongly suppressed by dimensional and microstructural constraints. Some strengthening mechanisms have proposed to explain the high strengths of these materials as their characteristic dimensions shrinking toward the nanoregime, e.g. (i) the Hall–Petch like strengthening relationship [8–10] applicable at the sub-micrometer length scales, (ii) the confined layer slip (CLS) mechanism [11–13] applicable at few to a few tens of nanometers length scales, and (iii) the interface barrier strength (IBS) mechanism [14,15] at a few nanometers length scales. A question naturally arises as to whether the fracture mode of the multilayers will be dependent on the strengthening mechanisms at the nanoscale length. Recently, Zhu et al. [16] suggested that the fracture mode of nanostructured Cu/Ta multilayers was directly related to the strengthening mechanism. They compared the damage behaviors of nanostructured Cu/Ta multilayers with λ = 10 nm and 250 nm and found that the 10 nm-multilayer exhibited shear-mode fracture while the 250 nm-multilayer fractured in opening mode [16]. Based on theoretical analyses of CLS and IBS, they claimed that the shear-mode and opening-mode fracture was associated with the strengthening mechanism of IBS and CLS, respectively. At the IBS-applicable regions (λ = 10 nm for Cu/Ta multilayers), the dislocation would transmit across the interface to cause a shear offset, finally resulting in shear-mode fracture. While at the CLS regions (λ = 250 nm for Cu/Ta multilayers), the dislocation glide is confined to one layer and no dislocation will transmit across the interface, the increasing local stress concentration ahead of the crack will cause an opening-mode fracture. However, the experiments in Zhu et al.'s work were incomplete because only two samples (equal individual layer thickness with λ = 10 nm and 250 nm) were examined. This makes their conclusion dubitable. In this paper, the variation in fracture mode of NMFs is focused, especially with respect to the change in strengthening mechanism. Extensive experiments are carried out to systematically investigate the damage behaviors in nanostructured Cu/Cr multilayers with a series of λ (at the same η) and a series of η (at the same λ), respectively. We draw a conclusion from careful analyses that the dominant factor controlling the fracture mode is the constraint effect of ductile phase on brittle phase, rather than the change in strengthening mechanism. Some theoretical analyses based on fracture mechanism are also given to quantitatively assess the constraint effect.

2. Experimental procedure

Two kinds of polyimide-supported Cu/Cr NMFs with total thickness about 500 nm were synthesized by means of direct current

* Corresponding authors. Tel.: +86 02982668695; fax: +86 02982663453.
E-mail addresses: lgsammer@mail.xjtu.edu.cn (G. Liu), junsun@mail.xjtu.edu.cn (J. Sun).

0921-5093/$ – see front matter © 2010 Elsevier B.V. All rights reserved.
doi:10.1016/j.msea.2010.12.054

(DC) magnetron sputtering at room temperature. The first ones have a constant modulation ratio η of 1 (η defined the ratio of Cr layer thickness h_{Cr} to Cu layer thickness h_{Cu}, $\eta = h_{Cr}/h_{Cu}$) but a wide range of modulation period λ ($\lambda = h_{Cr} + h_{Cu}$) from 10 to 250 nm. The second ones have a constant λ (λ = 25, 50 and 100 nm, respectively) but a wide range of η from 0.11 to 3.0. In film deposition, the first layer on the polyimide substrate was Cr and the last layer was Cu. The as-deposited Cu/Cr NMFs were annealed at 150 °C for 2 h to stabilize the microstructure and eliminate the residual stress. The X-ray diffraction (XRD) experiment was carried out using an improved Rigaku D/max-RB X-ray diffractometer with Cu Ka radiation and a graphite monochromator to determine the crystallographic texture and the residual stress by using "$\sin^2\psi$ method" [4,5]. Transmission electron microscopy (TEM) observation was performed using a JEM2100 high-resolution electron microscopy (HRTEM) with 200 kV accelerating voltages to observe the modulation structure and the interface structure.

Uniaxial tensile testing was performed using a Micro-Force Test System (MTS® Tytron 250) at a constant strain rate of $1 \times 10^{-4}\,s^{-1}$ at room temperature. All the samples have a total length of 65 mm and a gauge section of 30 mm in length and 4 mm in width and were strained to a certain magnitude about 10%. During tensile testing, the force and displacement were automatically recorded by machine and a high-resolution laser detecting system, respectively, which can be subsequently converted into stress–strain curve of the films by subtracting the load–displacement data of the pure substrate from the total ones of the systems [4,5,17]. When the intrinsic strain–stress curve of Cu/Cr NMFs is obtained after the subtraction treatment, the yield strength ($\sigma_{0.2}$) is determined as the 0.2% offset. In order to analyze the failure mechanism, tested Cu/Cr NMFs were cross-sectioned and characterized using a FEI Dual-Beam focused ion beam/scanning electron microscope (FIB/SEM). The fracture mode (e.g., opening fracture and shear fracture) was characterized by the fracture angle θ, which is defined as the angle between the macro-cracking direction and the horizontal direction. The values of θ are measured statistically based on the FIB cross-section images.

3. Results and discussion

3.1. Microstructure

The high-angle symmetrical XRD results revealed that the multilayers had a strong ⟨1 1 1⟩ out-of-plane texture components in Cu layers and a strong ⟨1 1 0⟩ out-of-plane texture components in Cr layers. The in-plane orientations are random in both the two layers. The residual stress has been measured by XRD using "$\sin^2\psi$ method", and were determined about 200 ± 100 MPa for all the annealed NMFs with different λ and η, which is far lower than their yield strength [4,5]. Typical cross-sectional views of some NMFs from the transmission electron microscopy (TEM) observations are displayed in Fig. 1, showing columnar grains in the Cu layers and ultra-fine nanocrystals in the Cr layers. The average grain sizes of both Cu and Cr scale with layer thickness. The selected area diffraction patterns (SADPs) indicates that all the NMFs exhibit a strong Kurdjumov–Sachs (K–S) orientation relationship in the growth

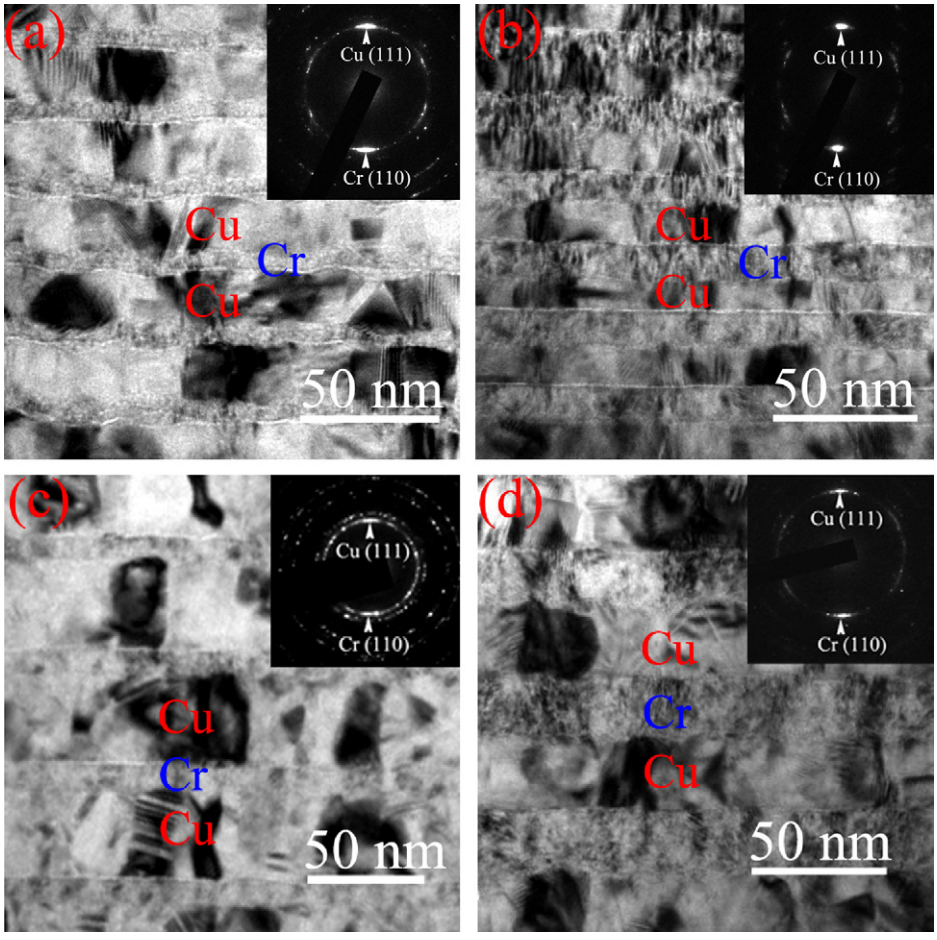

Fig. 1. Bright-field cross-sectional TEM micrographs showing typical microstructure of the Cu/Cr NMFs with different λ ((a) and (b): λ = 25 nm; (c) and (d): λ = 50 nm) and different η ((a) and (c): η = 0.33; (b) and (d): η = 1.0). Insert is the corresponding selected area diffraction patterns (SADPs).

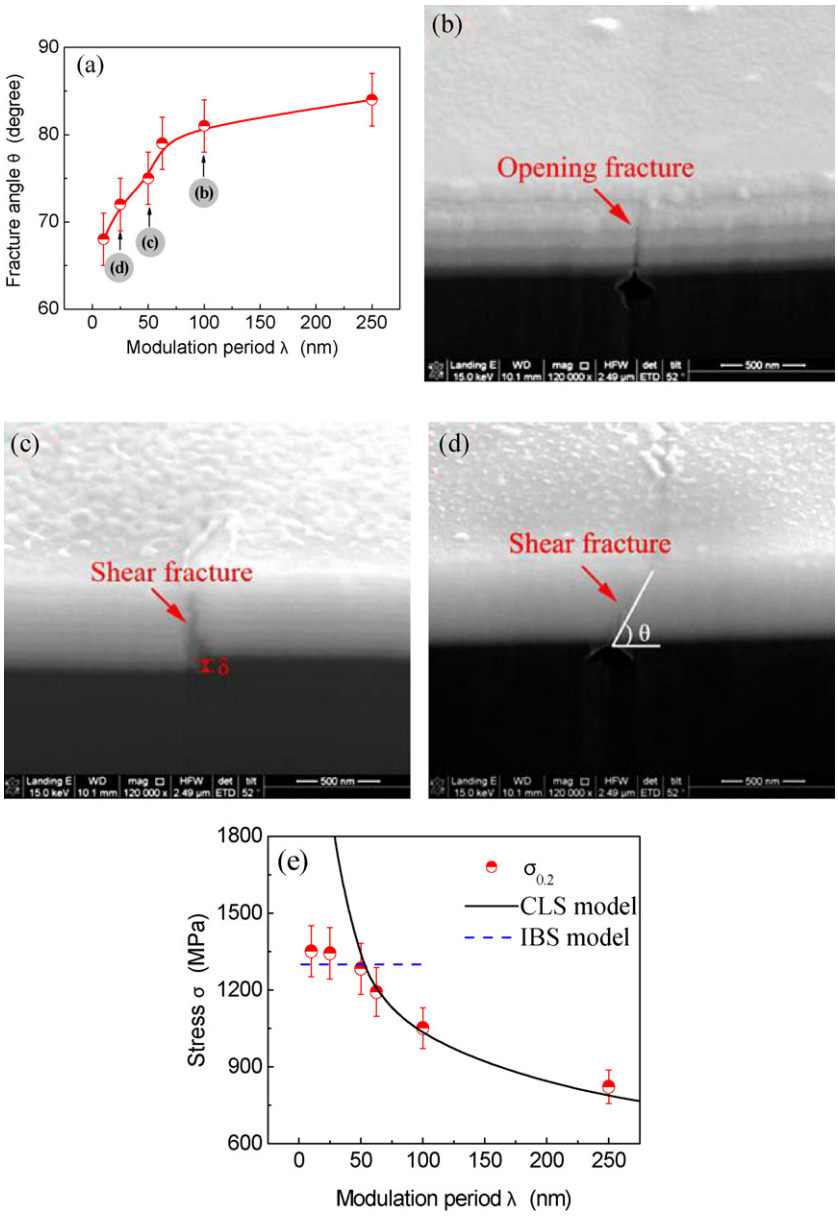

Fig. 2. (a) Dependence of θ on λ for the Cu/Cr NMFs with $\eta = 1$. The SEM cross-sectional images of (b) typically showing opening mode in Cu/Cr NMFs with $\lambda = 100$ nm, and (c) and (d) showing shear mode in the Cu/Cr NMFs with $\lambda = 50$ and 25 nm, respectively. (e) Dependence of $\sigma_{0.2}$ on λ for the Cu/Cr NMFs with $\eta = 1$. In (e), the solid curve (σ_{CLS}) is calculated from CLS model and the dash curve (σ_{IBS}) is from the IBS model.

direction: {1 1 1}Cu//{1 1 0}Cr; ⟨1 1 0⟩ > Cu// ⟨1 1 1⟩ Cr, except the one with $\lambda = 250$ nm showing random orientations in Cu layer and a {1 1 0} texture in Cr layer, consisting with the XRD results.

3.2. Modulation period dependent fracture behavior

We firstly examined the fracture behavior of NMFs with constant η of 1 but λ range spanning from 10 to 250 nm. Seen from Fig. 2(a), with λ decreased from 250 nm down to about 60 nm, the Cu/Cr NMFs exhibited opening fracture with $\theta \sim 83 \pm 3^\circ$, as typically shown in Fig. 2(b) the case of $\lambda = 100$ nm. Further reducing λ, the Cu/Cr NMFs inclined to fracture in shear mode fracture. The fracture angle gradually decreases down to about 70°. The images in Fig. 2(c) with $\theta \sim 75 \pm 3^\circ$ for $\lambda = 50$ nm and in Fig. 2(d) with $\theta \sim 72 \pm 3^\circ$ for $\lambda = 25$ nm clearly demonstrate the different fracture mode from that in Fig. 2(b). One can see that the present Cu/Cr NMFs with a smaller λ are more apt to fracture in a shear mode, essentially similar to observations in Cu/Nb nanolaminates tested by compression [18] and room temperature rolling [19], respectively. According to Zhu et al.'s suggestions [16], the change from opening- to shear-mode fracture in present Cu/Cr NMFs at critical $\lambda^{cri} \sim 60$ nm may be related to the change in strengthening mechanism from CLS to IBS.

As well known, the deformation of the NMFs is mainly controlled by the nucleation and motion of single dislocation in soft or ductile phase. The CLS model [5,11–13] involves the glide of single dislocation loop in soft phase bounded by two interfaces while the IBS model considers the interface cutting by single dislocation. When the CLS stress (σ_{CLS}) to drive the dislocation glide exceeds the IBS stress (σ_{IBS}) to drive the dislocation cross the interface, the strengthening mechanism will transmit from CLS to IBS model.

According to the CLS model, the needed σ_{CLS} to propagate a glide loop of Burgers vector b confined to the Cu layer is given as [5,13]:

$$\sigma_{CLS} = \frac{M\mu^* b \sin\varphi}{8\pi h_{Cu}} \left(\frac{4-\nu}{1-\nu}\right) \ln\left(\frac{\alpha h_{Cu}}{b \sin\varphi}\right) + \frac{f}{h_{Cu}} + \frac{\mu^* V_{Cr}\varepsilon}{m(1-\nu)} \quad (1)$$

where M is the Taylor factor, b is the length of the Burgers vector, φ is the angle between the slip plane and the interface, ν is the Poisson ratio for Cu, $\mu^* = \mu_{Cr} \cdot \mu_{Cu}/2(V_{Cr} \cdot \mu_{Cu} + V_{Cu} \cdot \mu_{Cr})$ is the mean shear modulus of Cu/Cr NMFs which can be estimated by the shear modulus μ_{Cu} and volume fraction V_{Cu} of the Cu layer and those of the Cr layer, α represents the core cut-off parameter, f is the characteristic interface stress of multilayer, ε is in-plane plastic strain and m is a strain resolution factor of the order of 0.5 for the active slip systems. On the other hand, σ_{IBS} is given by [14,15]:

$$\sigma_{IBS} = M\beta\mu^* \left(\zeta - \frac{b}{L}\right) + \frac{MRb\mu_{Cu}\sin\varphi}{4\pi r} \quad (2)$$

where β is Saada's constant, ζ is the lattice mismatch between interplanar spacing of {1 1 0}Cr and {1 1 1}Cu, r is the distance between the dislocation and interface, $L(L = b/\varepsilon$ [13]) is a parallel array of glide loops of spacing, $R = (\mu_{Cr} - \mu_{Cu})/(\mu_{Cr} + \mu_{Cu})$ and other symbols have the same meaning as before. Taking $M = 3.06$, $\mu_{Cu} = 48.3$ GPa, $\mu_{Cr} = 115.4$ GPa, $\nu = 0.343$, $b = 0.2556$ nm, $\alpha = 0.2$, $f = 3$ J/m^2, $\varepsilon = 1\%$ and $\varphi = 70.5^\circ$ into Eq. (1), and $\varphi = 70.5^\circ$, $\zeta = 2.3\%$, $\beta \approx 0.4$ and $r = 6b$ into Eq. (2), the dependence of σ_{CLS} and σ_{IBS} on λ ($\eta = 1$) is respectively calculated and plotted in Fig. 2(e). σ_{CLS} increases with reducing λ while σ_{IBS} is independent of λ. For the present NMFs, the intersection point of the σ_{IBS} line and σ_{CLS} curve at about 1.3 GPa yields a critical $\lambda^{cri} \sim 60$ nm. Below λ^{cri}, the needed σ_{CLS} exceeds σ_{IBS}, indicating that the interface cutting is more easy to operate. Above λ^{cri}, however, external stress drives the single dislocation pile-ups at the interfaces/grain boundaries to generate strong stress concentration to cause opening fracture. The predicted λ^{cri} for strengthening mechanism change agrees well with the experimentally measured λ^{cri} for fracture mode change. It seems that the fracture mode is simply controlled by the strengthening mechanism, supporting Zhu et al.'s conclusion [16]. However, only the NMFs with $\eta = 1$ have been examined up to now, just like in Zhu et al.'s work [16]. Below, we will see from the further examination on NMFs with a wide range of η that the dominant factor controlling the fracture mode is actually *not* the strengthening mechanism.

3.3. Modulation ratio dependent fracture behavior

Fig. 3(a) shows the experimentally determined θ at different η for three NMFs with $\lambda = 25$, 50, and 100 nm, respectively. As η decreases from 3 to 0.11, all the three NMFs exhibit θ monotonically reduced from $\sim 84 \pm 3^\circ$ to $\sim 52 \pm 4^\circ$, indicating the fracture mode ranging from opening (Fig. 3(c)) to shear one (Fig. 3(d)). Interestingly, the critical η for opening-to-shear mode change is almost the same ($\eta^{cri} \sim 1$) for the three NMFs, and the three NMFs have close θ especially when η larger than 2. In comparison, similar calculations are performed again using Eqs. (1) and (2), respectively, to reveal the theoretical influence of η on σ_{CLS}, σ_{IBS}, and η^{cri}. The calculation results are shown in Fig. 3(b). One can see that, although σ_{IBS} is independent of λ, σ_{CLS} depends remarkably on η. As a result, the intersection point η^{cri} between the σ_{IBS} and σ_{CLS} curves, is significantly λ-dependent, from $\eta^{cri} \sim 1.7$ at $\lambda = 100$ nm to $\eta^{cri} \sim 0.5$ at $\lambda = 25$ nm. Obviously, the prediction is inconsistent with experimental result of almost λ-free as mentioned above. This indicates that it is actually unreasonable to explain the opening-to-shear transition in fracture mode by referring to the change in strengthening mechanism. Below, a constraint effect from the ductile layer on the brittle layer is proposed to be the dominant factor controlling the opening-to-shear transition in fracture mode, which is quantitatively assessed by using a micromechanical model.

3.4. Fracture model

In present NMFs, microcracks are surely found to initiate within, and run across the Cr layer, which is the more brittle of the two constituent materials, due to the differences in elastic modulus and strength between the Cr and Cu layers. Further propagation of the

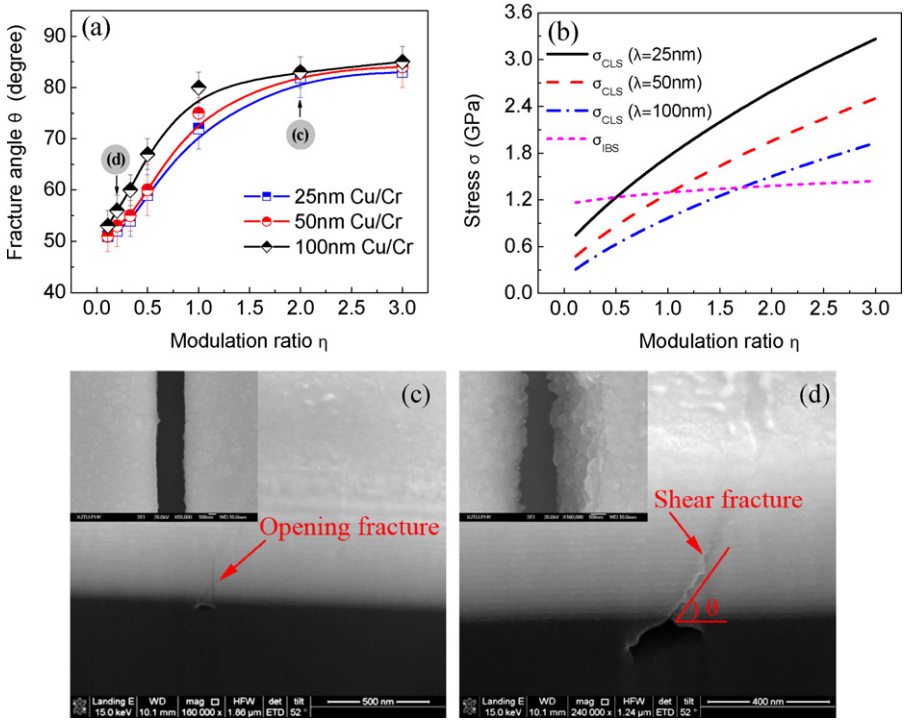

Fig. 3. (a) Dependence of θ on η for the Cu/Cr NMFs with $\lambda = 25$, 50 and 100 nm. (b) Theoretical estimation of the σ_{CLS} and the σ_{IBS} of the laminate composites with three different λ, showing a critical η above which the dislocation would transmit across the interface to cause a shear offset. Curves are guide to the eyes. The SEM cross-sectional images of (c) and (d) typically showing shear mode and opening mode, in $\lambda = 25$ nm Cu/Cr NMFs with $\eta = 0.2$ and $\eta = 2$, respectively. Insets show the corresponding SEM plan view image of the NMFs, which can be used to further demonstrate the shear and opening fracture mode.

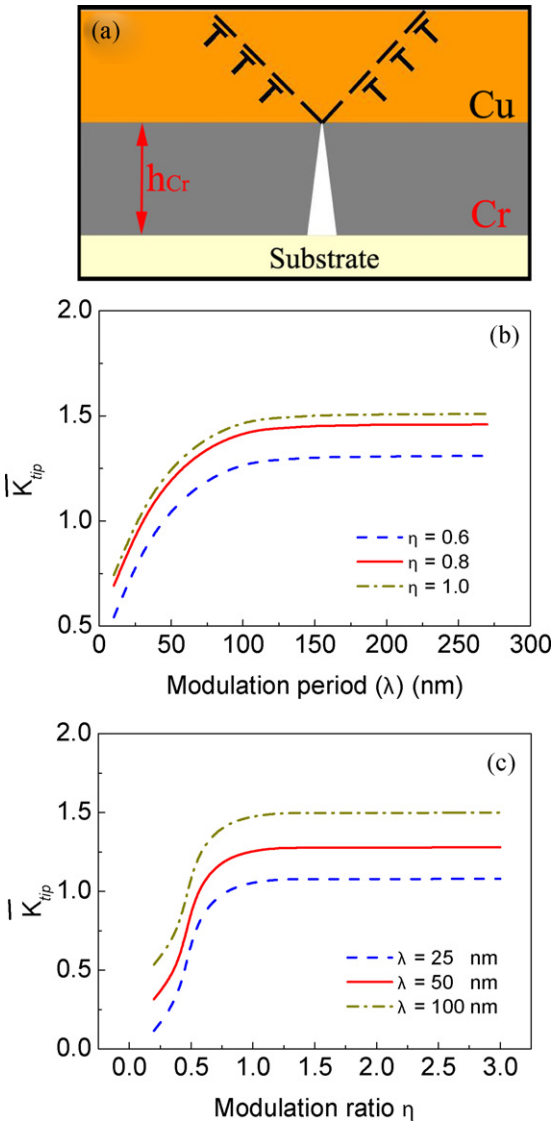

Fig. 4. (a) Sketch of the micromechanical fracture model. (b) Dependence of $\tilde{K}_{tip}$ on η as a function of λ. (c) Dependence of $\tilde{K}_{tip}$ on λ as a function of η.

microcracks is arrested by the more ductile Cu layers (Fig. 4(a)). Whether the microcracks can be stopped depends on two factors. The first is the intensity of stress/strain fields (ISF) ahead of the microcrack tip. ISF scales with $\sqrt{h_{Cr}}$ [20] as the size of the crack is approximately the thickness of the Cr layer. One can then expect that a smaller h_{Cr} is favorable for suppressing microcrack growth and yielding shear-mode fracture. This is the case in Fig. 2(a) with $\eta = 1$, where the decrease in λ means a reduction in h_{Cr} and so shear-mode fracture can be observed at smaller λ. The other factor is the shielding on microcrack propagation by the plastic deformation (dislocation) activities in Cu, which become rather limited when the h_{Cu} is too small. In other words, very thin Cu is less effective in hindering opening fracture. This is the case at lager η (Fig. 3(a)), where the Cu layer is much thinner compared with the Cr layer and so the NMFs fracture in opening mode.

The propagation of microcracks can be analyzed in the framework of fracture mechanics. A micromechanical fracture model [21] is subsequently employed to describe the constraint effect on the microcrack propagation. This model was dedicated to consider the effect of dislocation confinement on fracture behavior in laminates consisting of alternating ductile and brittle layers. Because the ductile layers have a size far below micron level, dislocations must be treated individually. As discussed above, microcrack is initiated in the brittle Cr layers and blocked by the interface, schematically shown in Fig. 4(a). Dislocations emitted from the microcrack tip have two effects: (i) blunt the crack-tip and thereby reduce the tensile stress at the crack tip, and (ii) pile up against an interface and send a back stress to the crack tip to hinder further dislocation emission. At a given load level, an equilibrium number (n) of dislocations exists, which can be given as [21]:

$$n = \frac{4\pi(1-\nu)}{\ln(\tilde{h}/\tilde{r})}\left(\frac{\tilde{K}_{app}\sqrt{\tilde{h}}}{A\sqrt{2\pi}}\sin\phi\cos\frac{\phi}{2} - \tilde{\gamma}\right) \tag{3}$$

where ϕ is the angle that the slip plane inclines from the interface (chosen as 45° without loss of generality); A is a factor slightly greater that unity; $\tilde{r} \approx 2.7\, r_0/b$ with r_0 being the effective core radius of dislocation and b the Burgers vector of the ductile material; $\tilde{K}_{app}$, $\tilde{h}$, and $\tilde{\gamma}$ are normalized value of far field mode I stress intensity K_{app}, maximum distance $h_\phi = h_M/\sin\phi$ that leading dislocation can travel, and surface energy γ, respectively:

$$\tilde{K}_{app} = \frac{K_{app}}{\mu\sqrt{b}}, \quad \tilde{h} = \frac{h_\phi}{b}, \quad \tilde{\gamma} = \frac{\gamma}{\mu b} \tag{4}$$

where μ is the shear modulus of the Cu layers. The tensile stress at the blunted crack tip ($\tilde{\sigma}_{tip} = \sigma_{tip}/\mu$) is related to n and $\tilde{K}_{app}$ as [21]:

$$\tilde{\sigma}_{tip}\sqrt{n} = 2\sqrt{\frac{2}{\pi}}\tilde{K}_{app}\left(1 - \frac{3\left(\sin\phi\cos(\phi/2)\right)^2}{\ln(\tilde{h}/\tilde{r})}\right) + \frac{12A}{\sqrt{\tilde{h}}\ln(\tilde{h}/\tilde{r})}\tilde{\gamma}\sin\phi\cos\frac{\phi}{2} \tag{5}$$

Increasing applied load, a competition between further dislocation emission and cleavage at the blunted crack tip will happen. When the microcrack tip tensile stress $\tilde{\sigma}_{tip}$ reaches the normalized cohesive strength of the material, $\tilde{\sigma}_c$ ($=\sigma_c/\mu$), fracture (cleavage) occurs in the ductile Cu layer and the pre-existed microcrack will propagate to form an opening fracture. Based on this criterion, the maximum number of dislocations emitted from the microcrack tip prior to cleavage (n_{max}) and the far field I stress intensity ($\tilde{K}_{app}$) can be resolved from Eqs. (3) and (5) in combination. The crack tip stress intensity ($\tilde{K}_{tip}$) is finally obtained as [21]:

$$\tilde{K}_{tip} = \tilde{K}_{app} - \frac{An}{(1-\nu)\sqrt{2\pi b\tilde{h}}}\frac{3}{2}\sin\phi\cos\phi \tag{6}$$

Calculations are performed and the results on $\tilde{K}_{tip}$ vs λ and $\tilde{K}_{tip}$ vs η are respectively obtained at a reasonable value $\tilde{\sigma}_c = 0.4$ that is applicable to ductile metals such as Cu [21]. The predicted results are shown in Fig. 4(b) and (c), respectively. In the $\tilde{K}_{tip}$ vs λ curves, the crack tip stress intensity notably reduces below $\lambda \sim 60$–80 nm at $\eta \sim 1$. Similarly in the $\tilde{K}_{tip}$ vs η curves, $\tilde{K}_{tip}$ sharply decreases below $\eta \sim 0.8$–0.9, within a wide range of λ from 25 to 100 nm. As well known, the larger crack tip stress intensity indicates that the microcrack is easier to propagate to form opening fracture. The predictions from Fig. 4(b) and (c) reveal that the transition in fracture mode, from opening to shear one, may be happened at the critical condition of $\lambda^{cri} \sim 60$–80 nm ($\eta \sim 1$) or $\eta^{cri} \sim 0.8$–0.9 (λ from 25 to 100 nm), which is in broad agreement with the present experimental results.

4. Conclusions

Both the nanostructured metallic multilayers with constant modulation ratio the ones with constant modulation period exhibited the transition of fracture mode from shearing to opening. The fracture mode in NMFs is then concluded to be controlled by

the constraint effect of ductile layer on brittle layer. The present experimental results and theoretical analyses can provide further understanding on the nanoscale damage of the NMFs, with which it is possible to artificially control the constituent phases or geometrical configures in NMFs to achieve advanced resistance to crack propagation.

Acknowledgements

This work was supported by the 973 Program of China (Grant No. 2010CB631003), the 111 Project of China (B06025) and the National Natural Science Foundation of China (50971097). GL thanks the support of Fundamental Research Funds for the Central Universities and GJZ thanks the support of the Program for New Century Excellent Talents in University (Grant No. NCET-10-0876).

References

[1] I. Bakonyi, L. Péter, Prog. Mater. Sci. 55 (2010) 107.
[2] Y.M. Wang, J. Li, A.V. Hamza, J.T.W. Barbee, Proc. Natl. Acad. Sci. U.S.A. 104 (2007) 11155.
[3] A. Donohue, F. Spaepen, R.G. Hoagland, A. Misra, Appl. Phys. Lett. 91 (2007) 241905.
[4] J.Y. Zhang, G. Liu, X. Zhang, G.J. Zhang, J. Sun, E. Ma, Scripta Mater. 62 (2010) 333.
[5] J.Y. Zhang, X. Zhang, G. Liu, G.J. Zhang, J. Sun, Scripta Mater. 63 (2010) 101.
[6] M.A. Phillips, B.M. Clemens, W.D. Nix, Acta Mater. 51 (2003) 3171.
[7] E. Arzt, Acta Mater. 46 (1998) 5611.
[8] G.S. Was, T. Foecke, Thin Solid Films 286 (1996) 1.
[9] A. Misra, H. Kung, Adv. Eng. Mater. 3 (2001) 217.
[10] P.M. Anderson, C. Li, Nanostruct. Mater. 5 (1995) 349.
[11] J.D. Embury, J.P. Hirth, Acta Metall. Mater. 42 (1994) 2051.
[12] M.A. Phillips, B.M. Clemens, W.D. Nix, Acta Mater. 51 (2003) 3157.
[13] A. Misra, J.P. Hirth, R.G. Hoagland, Acta Mater. 53 (2005) 4817.
[14] J.S. Koehler, Phys. Rev. B 2 (1970) 547.
[15] S.I. Rao, P.M. Hazzledine, Phil. Mag. A 80 (2000) 2011.
[16] X.F. Zhu, Y.P. Li, G.P. Zhang, J. Tan, Y. Liu, Appl. Phys. Lett. 92 (2008) 161905.
[17] R.M. Niu, G. Liu, C. Wang, G. Zhang, X.D. Ding, J. Sun, Appl. Phys. Lett. 90 (2007) 161907.
[18] N.A. Mara, D. Bhattacharyya, P. Dickerson, R.G. Hoagland, A. Misra, Appl. Phys. Lett. 92 (2008) 231901.
[19] A. Misra, R.G. Hoagland, J. Mater. Sci. 42 (2007) 1765.
[20] R.W. Hertzberg, Deformation and Fracture Mechanics of Engineering Materials, John Wiley & Sons Inc., 1989.
[21] K.J. Hsia, Z. Suo, W. Yang, J. Mech. Phys. Solids 42 (1994) 877.